

Self-passivation Causes the Different Fermi Level Pinning between Metal-Si and Metal-Ge Contacts

Ziying Xiang^{1,2}, Jun-Wei Luo^{1,2,*}, and Shu-Shen Li^{1,2}

¹*State Key Laboratory of Superlattices and Microstructures, Institute of Semiconductors, Chinese Academy of Sciences, Beijing 100083, China*

²*Center of Materials Science and Optoelectronics Engineering, University of Chinese Academy of Sciences, Beijing 100049, China*

*Email: jwluo@semi.ac.cn.

Abstract

Metal-Ge contacts possess much stronger Fermi level pinning (FLP) than metal-Si contacts, which is commonly believed to be due to Ge having a narrower bandgap and higher permittivity in the context of FLP caused by metal-induced gap states. Here, we show that both Ge and Si have a similar FLP strength if they adopt an identical interface chemical bonding configuration at the contact interface by performing first-principles calculations: Si and Ge have FLP factors of 0.16 and 0.11, respectively, if they adopt the same reconstructed bonding configuration and have FLP factors of 0.05 and 0, respectively, if they adopt the same non-reconstructed bonding configuration. We illustrate that Ge prefers the latter configuration at the contact interface, which has denser dangling-bond-induced surface states, and Si prefers the latter one, which has a self-passivation effect for reducing the dangling bond-induced interface states, to reproduce the experimental data. By revealing the significance of dangling bond-induced interface gap states on FLP, these findings shed new light on lowering the contact resistance for developing future Si CMOS technology.

With the continued scaling of Si complementary metal-oxide-semiconductor (CMOS) technology, the influence of source/drain contact resistance on the performance of metal-oxide-semiconductor field-effect transistors (MOSFETs) has been increasingly significant due to a smaller contact area and is now becoming a major bottleneck for advanced transistor performance scaling [1,2]. The International Roadmap for Device and Systems (IRDS) [3] sets a target for Si contact resistance below $10^{-9} \Omega\text{-cm}^2$, a goal that is challenging yet attainable. The challenge is primarily due to the strong Fermi level pinning (FLP) effect that causes a finite Schottky barrier height (SBH) $\Phi_{B,n}$ to form at the metal-Si interface. Meanwhile, the continued dimensional scaling of Si transistors also substantially degrades the channel mobility, which poses another great challenge and underscores the urgency to explore high-mobility channel materials, such as Ge [7], to sustain Moore's Law. Although Ge possesses superior carrier mobility as it has the highest hole mobility among all semiconductors, with electron mobility approximately three times higher than in Si [4], the extremely strong FLP effect at the metal-Ge interfaces [5] prevents it from replacing Si for developing next-generation low-power transistors [7]. Two-dimensional (2D) semiconductors as channel materials could enable transistors with sub-10 nm gate length while maintaining sufficiently small subthreshold swing and leakage current with ultimate body thickness down to one atomic layer but also suffer from poor source and drain contacts with a considerably large Schottky barrier due to the Fermi level pinning (FLP) effect [6-9]. The strength of the FLP for a given semiconductor is usually characterized by a pinning factor S [10]:

$$S = \frac{d\Phi_{B,n}}{d\phi_M}, \quad (1)$$

where ϕ_M is the work function (WF) of metals in contact. Experiments show that n-type Si has a pinning factor of $S = 0.15$ [11-14], and n-type Ge possesses $S = 0.02$ [5,14-16] the strongest FLP among semiconductors, manifesting the Fermi level firmly pinned at about 0.05 eV above the valence band maximum (VBM) and yielding a large constant n-type SBH (0.57 ± 0.07 eV) for the Ge-metal interface irrespective of the metal in contact [17]. Given the striking similarities in both crystal structure and electronic properties between Si and Ge, it is particularly interesting to note that Ge has much stronger pinning than Si, which makes Ge unlikely to replace Si for an NMOS channel [5,18].

The FLP effect is well recognized as arising from an interface dipole caused by charge redistribution at the metal-semiconductor (MS) interface due to the metal-induced gap states (MIGS) originating from the penetration of metal Bloch wave functions into the semiconductor band gap [12,19]. The occupation of the MIGS by electrons from the metal generates charges on the semiconductor surface, accompanied by induced opposing charges with the same amount on the metal surface. This charge redistribution establishes an interface dipole across the MS interface, resulting in a deviation of the metal Fermi level from its anticipated position as predicted by the

Schottky-Mott rule [20,21]. Based on the electrical double-layer model, the pinning factor S can be expressed as follows:

$$S = \left(1 + \frac{e^2 \delta_{it} D_{it}}{\epsilon_{it}} \right)^{-1} \quad (2)$$

Where D_{it} , δ_{it} , and ϵ_{it} are the density of gap states per unit area, effective distance away from the interface associated with the decay length of interface states, and effective dielectric constant at the interface region, respectively [22]. The MIGS model relates the D_{it} and δ_{it} to the magnitude of band gap E_g for a semiconductor [23,24], suggesting that Ge with a narrower band gap should exhibit a stronger FLP effect than Si due to higher density and larger decay length of MIGS [23]. The alleviation of the strong FLP by inserting an ultrathin dielectric insulator layer between the metal and semiconductor (Si and Ge) has further proved the MIGS model, regarding it can reduce the penetration of MIGS from the metal into the semiconductor [14,16,17,25]. However, the MIGS model has recently been questioned by both theoretical and experimental observations that show interface structure can strongly modify the SBH and FLP [26,27], which are unlikely to be explained in the context of the MIGS model since it regards FLP as purely an intrinsic property of the bulk semiconductors as it relies solely on bulk band gap or dielectric constant without considering the role of the specific structure of the interface. Therefore, the microscopic mechanisms underlying the strong FLP in the metal-semiconductor interfaces remain ambiguous. It prompts us to reconsider whether the difference in FLP between Ge and Si originates from their difference in interfacial bonding structures instead of intrinsic MIGS to explore more feasible ways to overcome the contact resistance challenge for advanced technology nodes.

In this work, by performing the first-principles calculations, we show that both Si and Ge have a similar FLP strength if they adopt the same interfacial bonding structure in contact with metals. Specifically, if a $p(2 \times 2)$ dimer reconstruction interfacial bonding configuration is adopted, the predicted pinning factor is $S = 0.16$ in excellent agreement with the well-established experimental data of $S = 0.15$ for n-type metal-Si interfaces [11,12]. However, this interfacial bonding configuration also results in Ge having a pinning factor $S = 0.11$ that is much larger than the experimental data $S = 0.02$ [5,14]. Interestingly, a $c(1 \times 1)$ non-reconstructed interfacial bonding structure reduces the pinning factor of Ge ($S = 0$) to reproduce the experimental data closely, but it gives rise to the pinning factor of Si dropping to $S = 0.05$. We show that the self-passivation of the interfacial Si dangling bonds renders the $p(2 \times 2)$ dimer reconstruction to have a smaller density of interface states and, thus, a larger S and a weaker FLP in comparison with the $c(1 \times 1)$ non-reconstructed interfacial bonding structure. We further illustrate that metal-Si interfaces prefer the $p(2 \times 2)$ dimer reconstruction as expected [28,29], but the metal-Ge interfaces prefer the $c(1 \times 1)$ non-reconstructed structure because it gains much less energy from the dimer reconstruction due to a longer bond length. We also demonstrate that we can substantially alleviate the FLP by increasing the pinning factor S to near 0.5 by fully passivating the interface dangling bonds with, e.g., hydrogen

atoms for both Si and Ge. These findings shed new light on overcoming the contact resistance for advanced technology nodes and new materials for future transistors.

It is well documented that the top-layer atoms of the clean Si(100) and Ge(100) surfaces will undergo pairing spontaneously, yielding reconstructions in $c(2\times 1)$, $c(4\times 2)$, $p(2\times 2)$, or $p(4\times 1)$ configurations [29,30]. The $p(2\times 2)$ dimer reconstruction has the lowest energy at low temperatures [31] and arises from the non-reconstructed ideal $c(1\times 1)$ surface termination by pairing the top-layer atoms along the [110] direction to form alternating buckled asymmetric dimers: one atom of the dimer displaces away from the surface (dimer-up atom), while the other moves inward (dimer-down atom) [32,33]. Therefore, we calculate the SBHs of the metal-Si and metal-Ge interfaces by considering metal deposition on the CMOS-compatible Si(100) and Ge(100) substrates, which are both in either $p(2\times 2)$ dimer reconstruction or ideal non-reconstructed $c(1\times 1)$ surface, using the first-principles density functional theory (DFT) with Heyd-Scuseria-Ernzerhof hybrid functional (HSE06) approach [34,35] as implemented in the PWmat code [36]. For more details, see the Supplemental Material (SM) [37] (see also references [38-40] therein).

Figure 1 shows the first-principles calculation results of the SBHs at the metal-Si and metal-Ge interfaces against the WF of metals in contact for both considered surface configurations compared with the well-established experimental data [5,11-15,41-48]. For the $p(2\times 2)$ dimer reconstruction, one can see from Fig. 1(a) that the first-principles calculated SBHs of the metal-Si interfaces agree with experimental measurements considering experimental data exhibiting a large scatter, but it is not true for metal-Ge interfaces. By fitting the theoretically predicted SBHs as a linear function of metal WF, we obtain a pinning factor $S = 0.16$ close to the experimentally reported value $S = 0.15$ [11,12] for metal-Si interfaces. The only exception is a slightly vertical shift (< 0.1 eV) in energy between two fitted curves, which may arise from the first-principles calculation uncertainties [40,49,50], e.g., the difference of the predicted electron affinity of bulk semiconductors from experimental data. Fortunately, these uncertainties do not affect our conclusions, which are based on the slope of the SBHs (see SM [37] for detailed SBHs). However, for the metal-Ge interfaces with the same $p(2\times 2)$ dimer reconstruction, the predicted pinning factor is $S = 0.11$, which is only 0.05 smaller than that of the metal-Si interfaces and thus is too large to account for the extremely strong FLP ($S = 0.02$) observed experimentally in the metal-Ge contacts [5,14,15], as shown in Fig. 1(c). Interestingly, as we change the interface configuration from the $p(2\times 2)$ dimer reconstruction to the ideal $c(1\times 1)$ non-reconstructed structure, the first-principles calculations reproduce the experimentally measured pinning factor of the metal-Ge contacts by substantially reducing the predicted pinning factor from $S = 0.11$ to $S = 0$ (Fig. 1(d)). Surprisingly, the ideal $c(1\times 1)$ non-reconstructed structure also remarkably reduces the pinning factor of the metal-Si interfaces to $S = 0.05$, manifesting that such interface configuration artificially makes Si have an extremely strong FLP comparable to Ge.

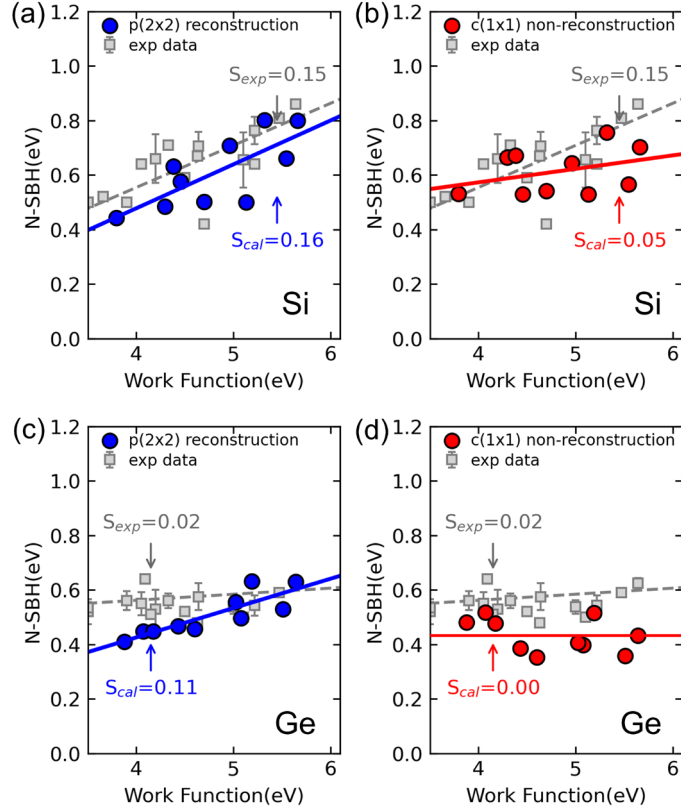


FIG. 1. Calculated n-type Schottky barrier height (N-SBH) of the metal-Si interfaces in (a) $p(2\times 2)$ dimer reconstruction interface configuration (b) $c(1\times 1)$ non-reconstructed interface configuration, respectively, and of the metal-Ge interfaces in (c) $p(2\times 2)$ dimer reconstruction interface configuration (d) $c(1\times 1)$ non-reconstructed interface configuration, respectively. Grey squares with error bars represent the experimental data [8,17,20-22,25-27,57-62].

Consequently, we show that the interfacial atomic bonding configuration plays a crucial role in determining the FLP strength since metal-Ge and metal-Si interfaces have similar FLP strength if they adopt an identical interface configuration. This implies that the metal-Si contacts prefer a reconstruction interface with a weaker FLP ($S = 0.15$) [11,12]. In contrast, the metal-Ge contacts prefer an ideal non-reconstructed interface with an extremely strong FLP ($S = 0.02$) [5,14,15]. This finding is strikingly in contrast with the common wisdom according to the MIGS models [12,14,19], which believes the FLP strength to be an intrinsic property of bulk semiconductors without the need to consider the detailed atom arrangements at the interface [14,19]. Evidence has been accumulated that metal deposition may destroy the reconstructed surface structure of the substrate [51,52], although both clean Si (001) and Ge (001) surfaces are predicted theoretically [29,31] and observed experimentally [53] to be stabilized in the $p(2\times 2)$ dimer reconstruction [31]. For instance, experiments have shown that Ba adsorption on the (001) Ge surface results in a change from the reconstruction surface to the $c(1\times 1)$ non-reconstructed surface [54].

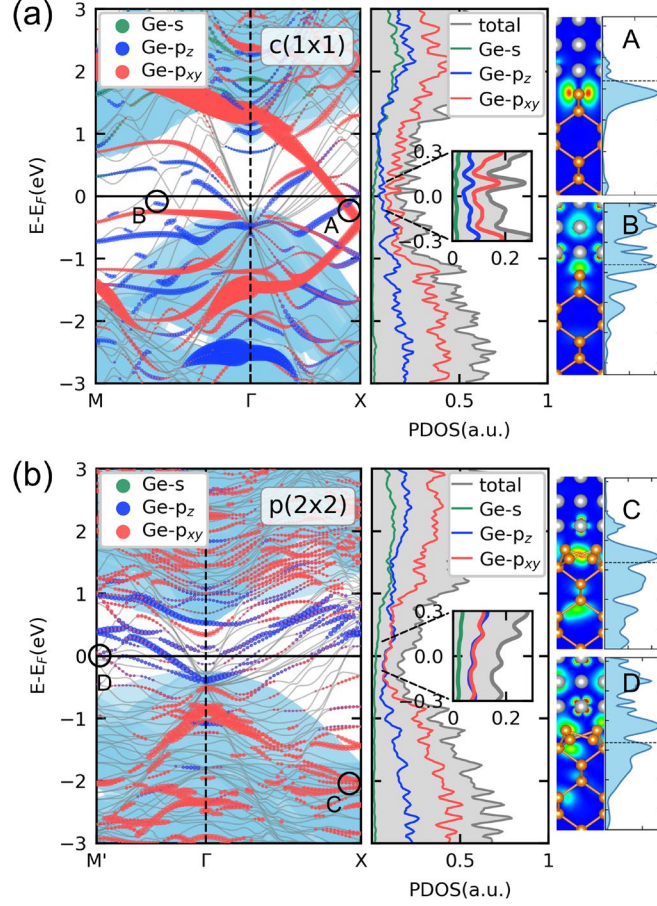


FIG. 2. The first-principles calculated interface band structure (marked by the gray lines in left panel) of the metal-Ge interface by projecting the Ag-Ge slab electronic states onto the first layer of Ge atoms and the projected density of states (PDOS) of all Ge layers (middle panel) for (a) $c(1 \times 1)$ non-reconstructed interface configuration and (b) $p(2 \times 2)$ dimer reconstruction interface configuration, respectively. In the left panels, the light-blue shadow represents the bulk band structure projected to the (100) surface BZ; the gray lines denote the interface band structure, and the colored dots represent Ge atomic orbitals with dot size accounting for the relative amplitude. In the middle panels, the insets zoom the PDOS near the Fermi level. The right panels show the partial charge distribution for typical interface states marked by black circles in the left panels. The orange spheres denote Ge atoms, and the silver spheres denote Ag atoms

We first attempt to reveal the microscopic mechanism responsible for the effect of interfacial atomic bonding configurations on the FLP strength before addressing why metal-Si contacts prefer a reconstruction interface but metal-Ge contacts prefer a non-reconstructed interface. To do so, we take Ag as a prototypical metal using an Ag/Ge supercell (containing 9 Ag layers and 13 Ge layers in the c -direction, as shown in Fig. SM-2 [37]) to examine the metal-Ge interface band structure by projecting the electronic states of the Ag-Ge interface on the top Ge layer. Notably, its projected density of states (PDOS) is more critical since the density of interface gap states D_{ii} governs the pinning factor S according to Eq. (2). Figure 2(a) shows that in the $c(1 \times 1)$ non-reconstructed

configuration Dirac-cone-like bands cross at the X-point, which, however, is absent in the $p(2\times 2)$ dimer reconstruction configuration, as shown in Fig. 2(b). It causes the total density of the interface states near the Fermi level to get reduced by changing the arrangement of the interfacial Ge atoms from the $c(1\times 1)$ non-reconstructed configuration to the $p(2\times 2)$ dimer reconstruction, which should account for a larger pinning factor S and weaker FLP strength observed in the latter interfacial configuration. Note that we can infer such a reduction in total density arising from the reduction of the partial density of p_{xy} orbital states near the Fermi level since the p_z orbital states have almost unaltered partial density. From the partial charge distribution of these interface gap states in real space, we can distinguish them either as metal-induced gap states (MIGS) [12,19] or dangling-bond-induced surface states (DBSS) [55]. Specifically, MIGS originates from the penetration of metal Bloch wave functions into the semiconductor band gap [12,19], resulting in charges distributing across the entire metal region and gradually decaying towards the semiconductor side [10]. Whereas DBSS emerges from the surface dangling bonds owing to the crystal lattice termination at the surface, and thus, its charges localize predominantly in the interface region and decay towards both sides [56]. Subsequently, we can identify Dirac-cone-like bands crossing at the X-point in the $c(1\times 1)$ non-reconstructed configuration as DBSS (see the right panel in Fig. 2(a)) and derived from the rehybridized p_{xy} states of surface Ge atoms (see the left panel in Fig. 2(a) and will be discussed below) [57,58]. We can further ensure the identification of the DBSS in Fig. 2(a) by referring to the surface states of the bare Ge surface (Fig. SM-5). We also find some interface gap states, e.g., indicated by B, arising from MIGS as expected (see the right panel in Fig. 2(a)). In contrast, in the $p(2\times 2)$ dimer reconstruction configuration, the in-plane dimerization of the Ge surface dangling bonds shifts most p_{xy} orbital states out of the bandgap to below the VBM or above the CBM and thus cannot form the Dirac-cone-like bands, as shown in Fig. 2(b). Specifically, these p_{xy} rehybridized states at the X point (indicated by C in the left panel of Fig. 2(b)) have a large amount of percentage distributed in the dimer region and resonate with Ge bulk states, yielding the surface resonance states [55,56]. We should note that p_z orbital states have no remarkable shift in energy and remain inside the band gap as changing the interface configurations. It implies that these DBSSs yielding the Dirac-cone-like bands cause the difference in the total density of interface gap states near the Fermi level and, thus, the FLP strength in the $c(1\times 1)$ non-reconstructed configuration from the $p(2\times 2)$ dimer reconstruction interface configuration.

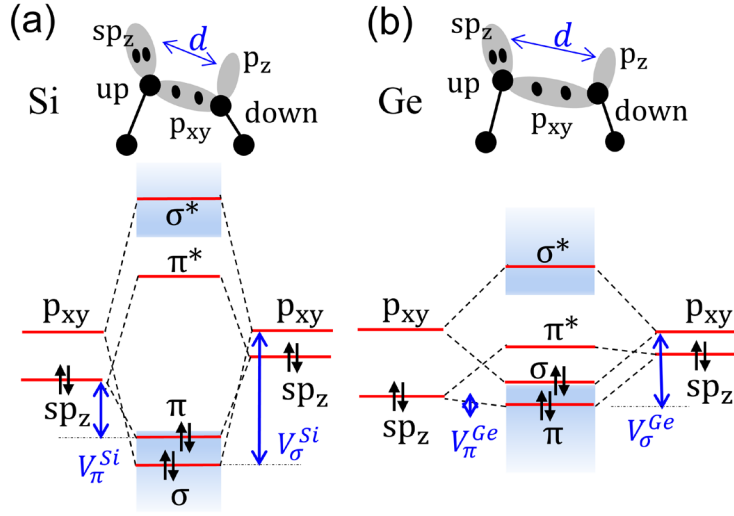


FIG. 3. Schematic diagram illustrating the coupling and the corresponding energy level shift of the rehybridize p_{xy} and sp_z states resulting from the dimerization in the $p(2 \times 2)$ dimer reconstruction configuration on (a) the Si(001) surface and (b) the Ge(001) surface. Here V and d represent the coupling of two hybrid orbitals and the distance between two surface atoms, respectively.

The ideal $c(1 \times 1)$ non-reconstructed (100) surface results from cutting parallel to the front surface of the cubic unit cell of the diamond structure, leaving two dangling bonds for each surface atom and one valence electron in each dangling bond. The sp_3 hybrid orbitals in each dangling bond will rehybridize into one p_{xy} and one sp_z states. The energy level of one p_{xy} states rises from the sp_3 level to the atomic level of the outermost p -orbitals ($3p$ in Si and $4p$ in Ge), and the sp_z state goes down to the average of the outermost s - and p -orbital atomic levels, respectively, as shown in Fig. SM-5(c) in the SM [37]. In each surface atom, the two valence electrons owned by the two dangling bonds transfer to the lower-lying rehybridized sp_z state to make it fully occupied and empty the higher-lying two rehybridized p_{xy} states. The coupling of higher-lying rehybridized p_{xy} states between adjacent surface atoms gives rise to Dirac-cone-like bands crossing at the X-point, being responsible for the p_{xy} -DBSS observed in the Ag-Ge interface, as shown in Fig. 2(a) (such as marked by A). When two adjacent surface atoms come closer to each other along the $[110]$ direction to form a dimer as a result of the transition from the $c(1 \times 1)$ non-reconstructed structure to the $p(2 \times 2)$ dimer reconstruction, their rehybridized p_{xy} states significantly overlap end to end and develop into the σ bonding and σ^* antibonding states, opening energy gap at the X-point for the Dirac-cone-like bands and moving from the band gap to below the VBM and above the CBM of the bulk semiconductor, respectively, as shown in Fig. 3. At the same time, their low-lying rehybridized sp_z states overlap to form π bonding and π^* antibonding states but with less energy shift. Note that the surface dimers would further tilt to have an asymmetric dimer structure with one atom up (named

dimer-up) and another atom down (named dimer-down), and the rehybridized sp_z state of the dimer-down atom exhibits more p_z character [28]. The valence electrons occupied the lower-lying rehybridized sp_z state in the $c(1\times 1)$ non-reconstructed structure transfer to the even lower σ and π bonding states, which further lowers the surface energy of the $p(2\times 2)$ dimer reconstruction and thus explains why both clean Si and Ge (001) surfaces stabilized in the $p(2\times 2)$ reconstruction at $T = 0$ K [31]. More details are given in Fig. SM-5 [37]. We also illustrate that the dimerization yields a self-passivation of the surface dangling bonds to reduce the density of the interface gap states, making the $p(2\times 2)$ dimer reconstruction have a weaker FLP than the $c(1\times 1)$ non-reconstructed configuration for MS interfaces.

the energy gain from the $p(2\times 2)$ dimer reconstruction of the (001) surface is governed by the energy separation between the bonding and antibonding states of the dimer, which is inversely proportional to the square of the dimer bond length [59] or lattice constant of bulk semiconductors. Because the lattice constant of Ge is 4.3% larger than that of Si, energy gain from the dimer reconstruction of the Ge(001) surface is less than that of the Si(001) surface, as schematically shown in Fig. 3. Therefore, the $p(2\times 2)$ dimer reconstruction is expected to be less stable in Ge than in Si, which has already been observed in experimental measurements [28,60,61]. Specifically, the weaker dimer bonding in the reconstructed Ge(100) surface has been confirmed experimentally by measuring the dimer bond length and the bonding strength [28], manifesting that the dimer bonds in Ge exhibit nearly a single bond character, while they in Si exhibit some double bond character. Subsequently, on the Ge(001) surface, metal deposition is more likely to perturb the energy level of the σ bonding state of rehybridized p_{xy} states to shift to above the π^* anti-bonding state of the rehybridized sp_z states. This energy reversal would result in no energy gain from the dimerization, causing the Ge(001) surface to return back to its ideal $c(1\times 1)$ non-reconstructed configuration (see bare surface band structure in Fig. SM-5 [37] for details). Therefore, it is now ready to understand that the metal-Si interfaces prefer the $p(2\times 2)$ interface reconstruction, and the metal-Ge interfaces prefer the $c(1\times 1)$ non-reconstructed structure.

We have illustrated that the dimerization-induced self-passivation of the surface dangling bonds is a key factor in reducing the interface gap states to alleviate the FLP in the metal-Si interface relative to metal-Ge interfaces. Considering the surface dangling bonds have not yet been fully passivated even in the $p(2\times 2)$ interface reconstruction, as shown in Fig. 2(b), we postulate that we can further alleviate the FLP by improving the passivation of the surface dangling bonds using, e.g., hydrogen atoms, which have been successfully used to shift all surface states out from the band gap on bare Si and Ge surfaces [62-64]. To validate this postulation, we have terminated each surface dangling bond by a hydrogen atom using a bond length of 1.51 Å for the Si-H bond and 1.56 Å for the Ge-H bond, a configuration found to be stable by Northrup [65] (see SM [37] for details). Figure 4(a) shows that the H-passivation remarkably increases the pinning factor S from 0.16 to 0.5 for the metal-Si interfaces, accompanied by a significant reduction in the interface gap states, as shown in

Fig. SM-6 [37]. This is also true for the metal-Ge interfaces as the pinning factor S increased from 0.11 to 0.45, as shown in Fig. 4(b). Consequently, we have explicitly demonstrated the critical role of the surface dangling bonds-induced interface gap states on the FLP in MS interfaces.

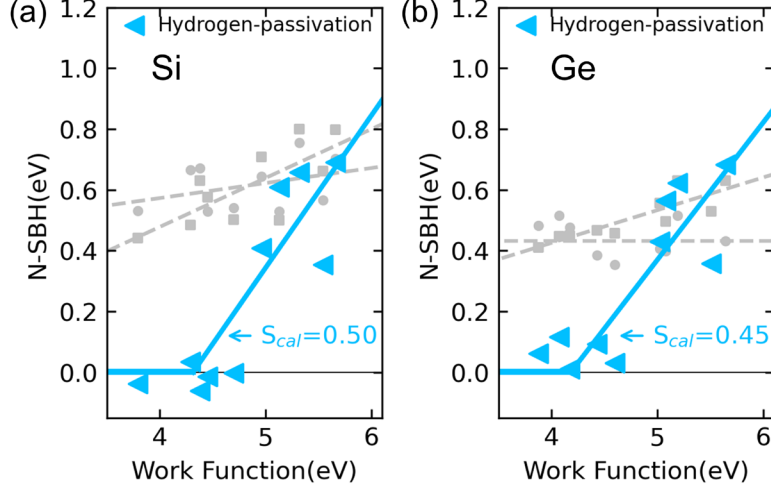


FIG. 4. First-principles predicted n-type Schottky barrier height (N-SBH) of (a) metal-Si and (b) metal-Ge interfaces after the complete passivation of the surface dangling bonds by hydrogen atoms. For comparison, the grey dots and squares represent the predicted values in the ideal $c(1\times 1)$ non-reconstructed configuration and the $p(2\times 2)$ dimer reconstruction, respectively, as shown in Fig. 1.

We note that both Nishimura et al. (2007) [14] and Kuzmin et al. (2016) [66] found that the modification of the atomic arrangement by altering the surface condition changes hardly the FLP strength or the pinning position and thus concluded that FLP of metal-Ge contacts is an intrinsic property and rises from MIGS. We must stress that their results are due to poor surface treatments, which may not effectively reduce the DBSS, considering Kuzmin's photoemission measurements showed little changes in the total surface component of core-level spectra by changing surface treatments [66].

On the other hand, even if we can fully passivate all DBSS, we still cannot make the pinning factor S approach the Schottky-Mott limit ($S = 1$). The residual FLP should arise from the commonly suggested MIGS [14,23]. Note that we do not disprove the significance of MIGS on the FLP in Ge and Si, although we attribute their different FLP to their different interface bonding configuration. The pinning factor S is consistently predicted to be slightly larger (within 0.05) in Si than that in Ge for the same configurations, as shown in Fig. 1, indicating the effect of MIGS on FLP since Si has a larger band gap than Ge and, thus, a smaller density of MIGS. Inserting an ultrathin insulator layer between the metal and the semiconductor has been introduced to alleviate the FLP by reducing the MIGS via suppressing the wave function tailing of the metal into the band gap of the semiconductor [18]. The ultrathin insulator insertion approach has been demonstrated to increase the pinning factor S of the metal-Si and metal-Ge contacts up to 0.24 [67] and 0.3 [16,68], respectively. The residual FLP should be due to the effect of DBSS.

In summary, we have revealed that the self-passivation of the interface dangling bonds is a primary factor in governing the different FLP strengths between the metal-Si and metal-Ge contacts since the former prefers the $p(2\times 2)$ dimer reconstruction interface and the latter prefers the $c(1\times 1)$ non-reconstructed interface structure. We have also demonstrated that utilizing hydrogen atoms to passivate the surface dangling bonds completely can further significantly increase the pinning factor S to 0.5, and the residual FLP should arise from the commonly suggested MIGS [14,23]. Thus, we shed new light on lowering the contact resistance for advanced technology nodes via modulating the FLP strength by passivating the interface bonding bonds without the need for an ultrathin dielectric layer [18,44], thereby avoiding the associated increase in tunnel resistance [16,69].

Acknowledgements

This work was supported by the CAS Project for Young Scientists in Basic Research under Grant No. YSBR-026, the Strategic Priority Research Program of the Chinese Academy of Sciences under Grant No. XDB43020000, and the National Natural Science Foundation of China (NSFC) under Grant Nos. 11925407 and 61927901.

References

- [1] G. Yeric, in *2015 IEEE International Electron Devices Meeting (IEDM)* (IEEE, Washington, DC, 2015), pp. 1.1.1.
- [2] S. Datta, W. Chakraborty, and M. Radosavljevic, *Science* **378**, 733 (2022).
- [3] International Roadmap for Devices and Systems (IRDS 2022), 2022.
- [4] R. Pillarisetty, *Nature* **479**, 324 (2011).
- [5] A. Dimoulas, P. Tsipas, A. Sotiropoulos, and E. K. Evangelou, *Appl. Phys. Lett.* **89**, 252110 (2006).
- [6] Y. Liu *et al.*, *Nature* **557**, 696 (2018).
- [7] Y. Wang *et al.*, *Nature* **568**, 70 (2019).
- [8] J. Jiang, L. Xu, C. Qiu, and L.-M. Peng, *Nature* **616**, 470 (2023).
- [9] W. Li *et al.*, *Nature* **613**, 274 (2023).
- [10] R. T. Tung, *Appl. Phys. Rev.* **1**, 011304 (2014).
- [11] C. R. Crowell, W. G. Spitzer, L. E. Howarth, and E. E. LaBate, *Phys. Rev.* **127**, 2006 (1962).
- [12] V. Heine, *Phys. Rev.* **138**, A1689 (1965).
- [13] W. Mönch, *Surf Sci.* **21**, 443 (1970).
- [14] T. Nishimura, K. Kita, and A. Toriumi, *Appl. Phys. Lett.* **91**, 123123 (2007).
- [15] T. Nishimura, T. Yajima, and A. Toriumi, *Appl. Phys. Express* **9**, 081201 (2016).
- [16] T. Nishimura, *Electronics* **11** (2022).
- [17] W. Mönch, *J. Appl. Phys.* **111** (2012).
- [18] Y. Zhou, M. Ogawa, X. Han, and K. L. Wang, *Appl. Phys. Lett.* **93**, 202105 (2008).

- [19] J. Tersoff, Phys. Rev. Lett. **52**, 465 (1984).
- [20] N. F. Mott, Proc. R. Soc. London, Ser. A **171**, 27 (1939).
- [21] W. Schottky, Z. Phys. **113**, 367 (1939).
- [22] A. M. Cowley and S. M. Sze, J. Appl. Phys. **36**, 3212 (1965).
- [23] X. Luo, T. Nishimura, T. Yajima, and A. Toriumi, Appl. Phys. Express **13**, 031003 (2020).
- [24] J. Ihm, S. G. Louie, and M. L. Cohen, Phys. Rev. Lett. **40**, 1208 (1978).
- [25] T. Nishimura, K. Kita, and A. Toriumi, Appl. Phys. Express **1**, 051406 (2008).
- [26] R. T. Tung, Phys. Rev. Lett. **52**, 461 (1984).
- [27] R. T. Tung and L. Kronik, Phys. Rev. B **103**, 085301 (2021).
- [28] P. Krüger and J. Pollmann, Phys. Rev. Lett. **74**, 1155 (1995).
- [29] A. Ramstad, G. Brocks, and P. J. Kelly, Phys. Rev. B **51**, 14504 (1995).
- [30] S. D. Kevan, Phys. Rev. B **32**, 2344 (1985).
- [31] H. J. W. Zandvliet, G. P. M. Poppe, C. M. J. Wijers, and A. v. Silfhout, Solid State Commun. **71**, 63 (1989).
- [32] J. Ihm, D. H. Lee, J. D. Joannopoulos, and J. J. Xiong, Phys. Rev. Lett. **51**, 1872 (1983).
- [33] M. Needels, M. C. Payne, and J. D. Joannopoulos, Phys. Rev. Lett. **58**, 1765 (1987).
- [34] J. Heyd, G. E. Scuseria, and M. Ernzerhof, J. Chem. Phys. **118**, 8207 (2003).
- [35] J. Paier, M. Marsman, K. Hummer, G. Kresse, I. C. Gerber, and J. G. Angyan, J. Chem. Phys. **124**, 154709 (2006).
- [36] W. Jia, Z. Cao, L. Wang, J. Fu, X. Chi, W. Gao, and L.-W. Wang, Comput. Phys. Commun. **184**, 9 (2013).
- [37] See Supplemental Material at [url], which includes Refs. [38-40], for structure and calculation details, for more band structure information.
- [38] S. Ciraci and I. P. Batra, Surf Sci. **178**, 80 (1986).
- [39] K. Y. Tse and J. Robertson, Phys. Rev. Lett. **99**, 086805 (2007).
- [40] M. Mrovec, J. M. Albina, B. Meyer, and C. Elsässer, Phys. Rev. B **79**, 245121 (2009).
- [41] S. Kurtin, T. C. McGill, and C. A. Mead, Phys. Rev. Lett. **22**, 1433 (1969).
- [42] S. M. Sze, Y. Li, and K. K. Ng, *Physics of semiconductor devices* (John Wiley & Sons, Hoboken, 2007).
- [43] D. R. Lide, *CRC handbook of chemistry and physics* (CRC press, Boca Raton, 2004).
- [44] R. R. Lieten, S. Degroote, M. Kuijk, and G. Borghs, Appl. Phys. Lett. **92**, 022106 (2008).
- [45] Y. Zhou, W. Han, Y. Wang, F. Xiu, J. Zou, R. K. Kawakami, and K. L. Wang, Appl. Phys. Lett. **96**, 102103 (2010).
- [46] A. Thanailakis and D. C. Northrop, Solid-State Electron. **16**, 1383 (1973).
- [47] H. B. Michaelson, J. Appl. Phys. **48**, 4729 (1977).
- [48] G. N. Derry, M. E. Kern, and E. H. Worth, J. Vac. Sci. Technol. A **33** (2015).
- [49] L. Lin, Y. Guo, and J. Robertson, Appl. Phys. Lett. **101**, 052110 (2012).
- [50] Q. Wang, Y. Shao, and X. Shi, J. Chem. Phys. **152** (2020).
- [51] L. H. Chan and E. I. Altman, Phys. Rev. B **66**, 155339 (2002).
- [52] O. Gurlu, H. J. W. Zandvliet, B. Poelsema, S. Dag, and S. Ciraci, Phys. Rev. B **70** (2004).

- [53] C. B. Duke, Chem. Rev. **96** (1996).
- [54] A. Cattoni, R. Bertacco, M. Riva, M. Cantoni, F. Ciccacci, H. Von Känel, and G. J. Norga, Mater. Sci. Semicond. Process. **9**, 701 (2006).
- [55] V. Heine, Surf Sci. **2**, 1 (1964).
- [56] H. Lüth, *Solid surfaces, interfaces and thin films* (Springer, Berlin, 2001).
- [57] J. A. Appelbaum, G. A. Baraff, and D. R. Hamann, Phys. Rev. B **11**, 3822 (1975).
- [58] L. D. Santis and R. Resta, Solid State Commun. **111**, 583 (1999).
- [59] W. A. Harrison, *Elementary electronic structure* (World Scientific, Singapore, 2004).
- [60] W. Stigler, P. Pavone, and J. Fritsch, Phys. Rev. B **58**, 13686 (1998).
- [61] A. A. Stekolnikov, J. Furthmüller, and F. Bechstedt, Phys. Rev. B **65**, 115318 (2002).
- [62] M. Rohlfing, P. Krüger, and J. Pollmann, Phys. Rev. B **54**, 13759 (1996).
- [63] I. Marri, M. Amato, M. Bertocchi, A. Ferretti, D. Varsano, and S. Ossicini, Phys Chem Chem Phys **22**, 25593 (2020).
- [64] M. Çakmak and G. P. Srivastava, Phys. Rev. B **60**, 5497 (1999).
- [65] J. E. Northrup, Phys. Rev. B **44**, 1419 (1991).
- [66] M. Kuzmin, P. Laukkanen, J. Mäkelä, M. Tuominen, M. Yasir, J. Dahl, M. P. J. Punkkinen, and K. Kokko, Phys. Rev. B **94**, 035421 (2016).
- [67] A. Agrawal *et al.*, Appl. Phys. Lett. **104** (2014).
- [68] M. Kobayashi, A. Kinoshita, K. Saraswat, H.-S. P. Wong, and Y. Nishi, J. Appl. Phys. **105**, 023702 (2009).
- [69] A. Agrawal, N. Shukla, K. Ahmed, and S. Datta, Appl. Phys. Lett. **101**, 042108 (2012).

Self-passivation Causes the Different Fermi Level Pinning between Metal-Si and Metal-Ge

Contacts

SUPPLEMENTAL MATERIAL

Ziying Xiang^{1,2}, Jun-Wei Luo^{1,2,*}, and Shu-Shen Li^{1,2}

¹*State Key Laboratory of Superlattices and Microstructures, Institute of Semiconductors,
Chinese Academy of Sciences, Beijing 100083, China*

²*Center of Materials Science and Optoelectronics Engineering, University of Chinese
Academy of Sciences, Beijing 100049, China*

*Email: jwluo@semi.ac.cn.

Modeling and computation details:

Metal-Si (metal-Ge) interfaces in the (100) orientation consist of at least 13 atomic layers of Si (Ge) and 9 layers of metals. We selected 10 metals including Ag, Au, Pt, Ta, Mg, Cu, Ir, Pd, Rh, and Ti. Our primary goal is to investigate the trends in the Schottky barrier height (SBH) and Fermi level pinning (FLP) strength variations, which are primarily governed by the metal work function (WF) rather than specific metal structure arrangements. To maintain consistency, metals with face-centered cubic structures were selected despite potential discrepancies in experimental phase structures. We kept the lateral lattice parameters of Si (Ge) slabs fixed to their calculated equilibrium bulk constants, and we rotated all the metal lattices by 45° and applied lateral strain to match the lattice parameters of Si (Ge) slabs. This approach ensures uniformity in interface atomic structures across all interfaces. Given the alternations in metal lattice parameters, we recalculated the corresponding new WF of the metals (similar calculations can also be found in the previous studies [1,2]). Although the calculated WFs differ from experimental values, this does not affect our analysis, as our primary focus is on the pinning factor S , which is determined by the rate of change of SBH with respect to WF, rather than the WF of an individual metal. Further calculation details are provided in Table SM-I and Table SM-II.

Figure SM-1 presents the optimized surface structures of three configurations (only the Ge surfaces are shown, as the Si surfaces are similar). For both the $c(1\times 1)$ non-reconstructed configuration and the $p(2\times 2)$ dimer reconstruction configuration, we tested the preferred bonding configuration, which was found to be at the hollow site. For the hydrogen-passivated structure, we

selected the 2×1 monohydride phase, known for its stability in hydrogen adsorption [3,4]. The preferred bonding configuration shifted to the top site. All surface structures were optimized using PBE functionals. We also optimized the displacements between the metal and semiconductor slabs to minimize the total energy. To better understand the correlation between the FLP effect and the ideal interface bonding structure, we fixed all the atomic positions. This strategy allowed us to control for additional variables that typically arise during atomic relaxation, thereby avoiding the complexity, diversity, and non-repeatability of real interface structures. For instance, in actual experiments, varying preparation temperatures can alter the interface atomic arrangement, leading to changes that are non-repeatable. Additionally, relaxation can significantly modify metal surface structures, potentially altering the originally calculated WF and leading to discrepancies with the calculated SBH. By isolating these factors, we could more clearly identify the impact of the interface bonding structure on the SBH and FLP.

In bulk calculation with HSE functional [5,6], we performed band structure calculation with dense reciprocal space grids of $10\times 10\times 10$ and adjusted the mixing coefficient α to obtain the correct experimental band gap (For Si, when $\alpha=0.25$, $E_g=1.17\text{eV}$) and for Ge, when $\alpha=0.18$, $E_g=0.67\text{eV}$). In the supercell calculations, considering the computational cost of HSE functional calculation, we used reciprocal space grids of $4\times 4\times 1$ in the self-consistent calculation, and $10\times 10\times 1$ in the following non-self-consistent calculations.

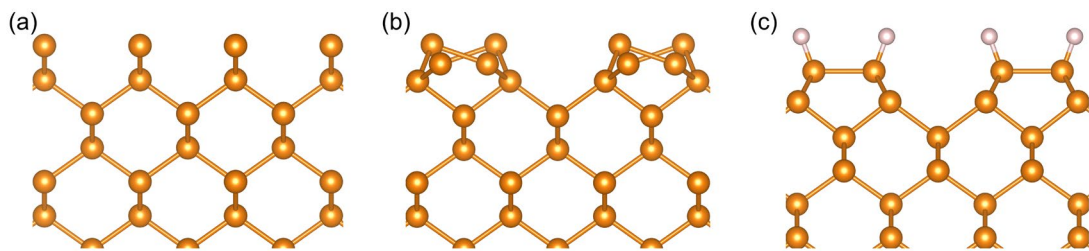


Fig. SM-1. Optimized structures of Ge(100) surface with (a) $c(1\times 1)$ non-reconstructed configuration, (b) $p(2\times 2)$ dimer reconstruction configuration and (c) hydrogen-passivated configuration. The orange and pink spheres represent Ge and H atoms, respectively.

Table SM-I. Calculated metal equilibrium lattice parameters a_M , the lattice mismatch between the metals and Si (Ge), the experimental work function (exp WF) [7,8], and the calculated work function (cal WF). Each metal lattice is rotated by 45° to better match the substrate lattice. The negative values of lattice mismatch indicate that the rotated metals have smaller lattice parameters compared to Si (Ge). The cal WFs are adjusted with the lattice parameters equal to the lattice parameter of Si ($a_{Si}=5.44 \text{ \AA}$) and Ge ($a_{Ge}=5.62 \text{ \AA}$), respectively. The exp WFs listed in the last column are not all obtained from the crystalline samples in the (100) orientation, with some being from polycrystalline samples.

Metal	a_M (\AA)	Si		Ge		exp WF (eV)
		lattice mismatch (%)	cal WF (eV)	lattice mismatch (%)	cal WF (eV)	
Ag	4.14	7.63	4.29	4.16	4.07	4.26
Au	4.15	7.8	5.12	4.33	5.08	5.10
Pt	3.94	2.27	5.66	-1.03	5.64	5.65
Ta	4.21	9.47	4.7	5.95	4.6	4.25
Mg	4.51	17.13	3.8	13.36	3.88	3.66
Cu	3.57	-7.27	4.46	-10.25	4.43	4.65
Ir	3.83	-0.51	5.54	-3.71	5.51	5.27
Pd	3.93	2	5.32	-1.28	5.19	5.12
Rh	3.79	-1.51	4.96	-4.68	5.02	4.98
Ti	4.1	6.59	4.38	3.15	4.17	4.33

Table SM-II. The calculated n-type Schottky barrier height (N-SBH) data of 10 metal-Si (Ge) contacts in three different interface configurations.

Metal	exp WF (eV)	N-SBH (eV)					
		Si			Ge		
		$c(1\times 1)$	$p(2\times 2)$	H	$c(1\times 1)$	$p(2\times 2)$	H
Ag	4.26	0.67	0.49	0.03	0.51	0.42	0.11
Au	5.1	0.53	0.50	0.61	0.40	0.49	0.56
Pt	5.65	0.70	0.80	0.69	0.43	0.63	0.68
Ta	4.25	0.56	0.57	0	0.37	0.51	0.03
Mg	3.66	0.54	0.46	-0.04	0.49	0.44	0.06

Cu	4.65	0.52	0.55	-0.01	0.37	0.43	0.09
Ir	5.27	0.58	0.71	0.35	0.37	0.57	0.36
Pd	5.12	0.77	0.83	0.66	0.52	0.64	0.62
Rh	4.98	0.64	0.71	0.41	0.41	0.56	0.43
Ti	4.33	0.67	0.64	-0.06	0.47	0.42	0.01

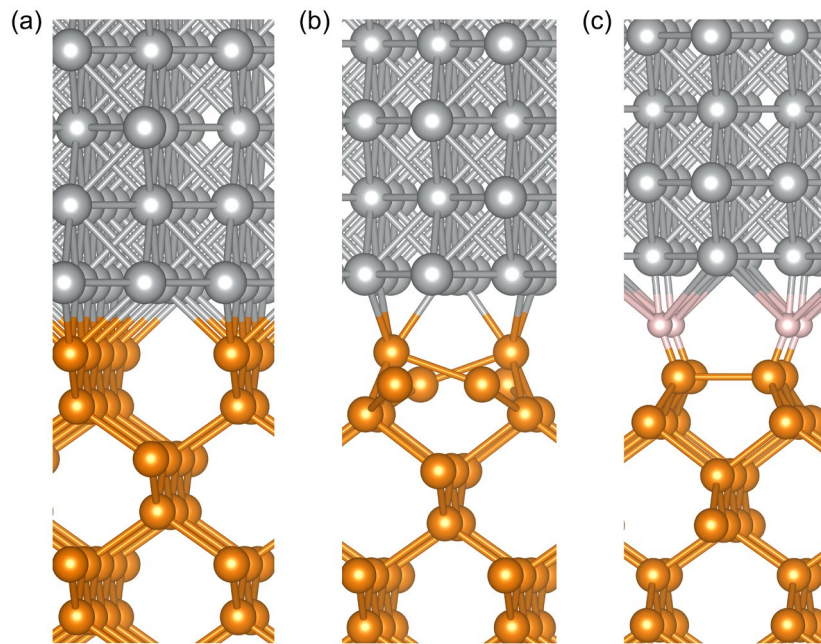


Fig. SM-2. Ag-Ge interface structure of (a) $c(1\times 1)$ non-reconstructed configuration, (b) $p(2\times 2)$ dimer reconstruction configuration and (c) hydrogen-passivated configuration. The orange, pink and silver spheres represent Ge, H, and Ag atoms, respectively.

More band structure information:

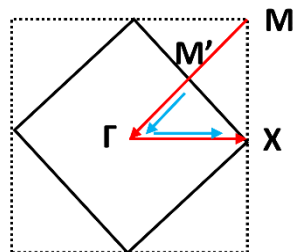


Fig. SM-3. The surface Brillouin zone and high symmetry points of $c(1\times 1)$ (outer dashed line and red arrow) and $p(2\times 2)$ (inner straight line and blue arrow) unit cells.

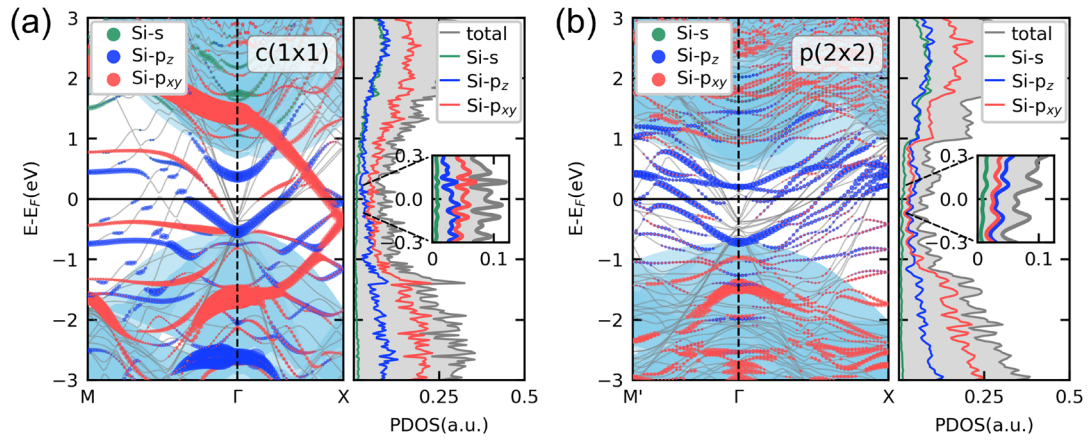


Fig. SM-4. Ag-Si interface band structure projected on the first layer of Si atoms and the sum of projected density of states (PDOS) of all Si atoms in (a) $c(1 \times 1)$ non-reconstructed configuration and (b) $p(2 \times 2)$ dimer reconstruction configuration.

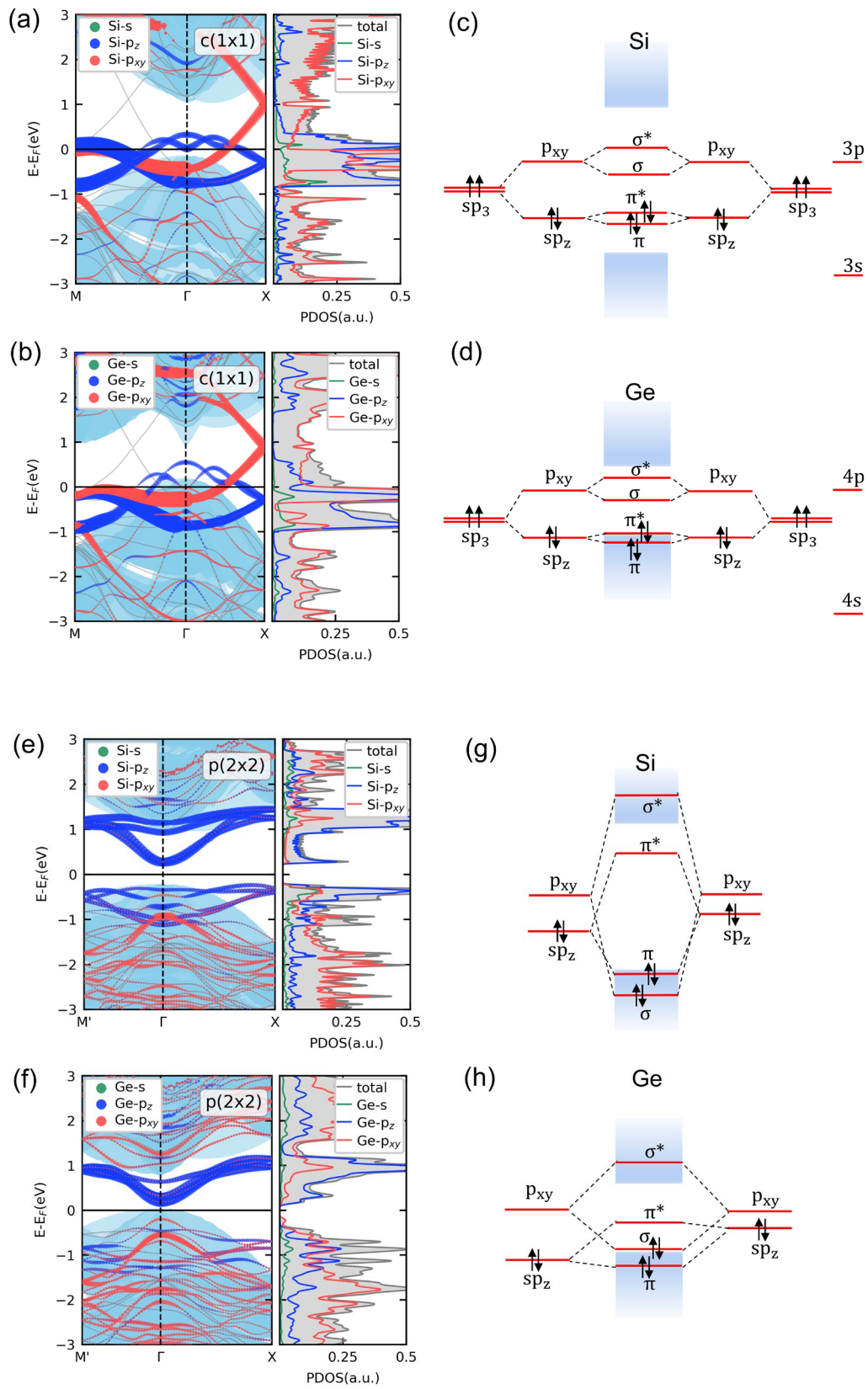


Fig. SM-5. Band structure and density of states projected on the first atomic layer of bare Si and Ge

surface with two different configurations: $c(1\times 1)$ non-reconstructed configuration in (a) Si and (b) Ge with schematic diagrams illustrating the corresponding energy levels in (c) and (d), $p(2\times 2)$ dimer reconstruction configuration in (e) Si and (f) Ge with schematic diagrams illustrating the corresponding energy levels in (g) and (h).

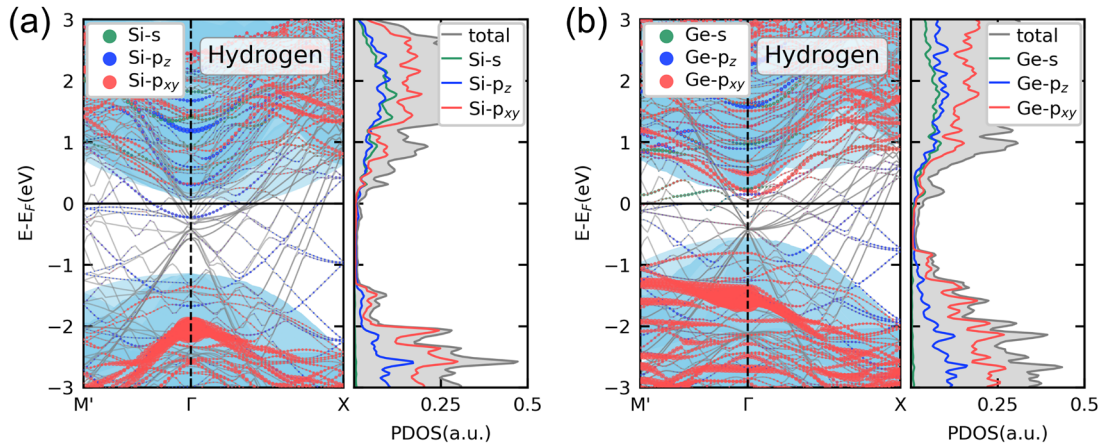


Fig. SM-6. (a) Ag-Si and (b) Ag-Ge interface band structure projected on the first layer of semiconductor atoms and the sum of projected density of states (PDOS) of all semiconductor atoms in hydrogen-passivated configuration.

References

- [1] M. Mrovec, J. M. Albina, B. Meyer, and C. Elsässer, *Phys. Rev. B* **79**, 245121 (2009).
- [2] K. Y. Tse and J. Robertson, *Phys. Rev. Lett.* **99**, 086805 (2007).
- [3] S. Ciraci and I. P. Batra, *Surf. Sci.* **178**, 80 (1986).
- [4] J. E. Northrup, *Phys. Rev. B* **44**, 1419 (1991).
- [5] J. Heyd, G. E. Scuseria, and M. Ernzerhof, *J. Chem. Phys.* **118**, 8207 (2003).
- [6] J. Paier, M. Marsman, K. Hummer, G. Kresse, I. C. Gerber, and J. G. Angyan, *J. Chem. Phys.* **124**, 154709 (2006).
- [7] H. B. Michaelson, *J. Appl. Phys.* **48**, 4729 (1977).
- [8] G. N. Derry, M. E. Kern, and E. H. Worth, *J. Vac. Sci. Technol. A* **33** (2015).